Electronic supplementary information (ESI)

Selective Tandem Electroreduction of Nitrate to Nitrogen via Copper-Cobalt Based Bimetallic Hollow Nanobox Catalysts

Ruoqing Wu, Tingting Yan, Kai Zhang, Zhenlin Wang, Haiyan Duan, Qiuying Yi, Danhong Cheng,* and Dengsong Zhang*

International Joint Laboratory of Catalytic Chemistry, Department of Chemistry, College of Sciences, Shanghai University, Shanghai 200444, P. R. China.

*E-mail: dszhang@shu.edu.cn (DS Zhang); cdh@shu.edu.cn (DH Cheng).

The Supporting Information includes 34 Pages, 14 Figures and 9 Tables.

Table of Contents

Materials and reagents

All of the chemicals and reagents were of analytical grade and used as received without any further purification. Cobalt nitrate hexahydrate ($Co(NO_3)_2·6H_2O$), copper nitrate trihydrate ($Cu(NO_3)_2·3H_2O$), hexadecyl trimethyl ammonium bromide (CTAB), sodium nitrate ($NaNO_3$), sodium sulfate (Na_2SO_4) and commercial CuO were purchased from Sinopharm Chemical Reagent Co. Ltd (Shanghai, China). 2−methylimidazole and poly tetra fluoroethylene (PTFE) were obtained from Aladdin (Shanghai, China).

Experimental section

Synthesis of ZIF−67 nanocube: The ZIF−67 nanocube were synthesized mainly according to the reference,[1] and made the appropriate adjustment basing on the actual situation. In a typical synthesis, 580 mg of $Co(NO_3)_2·6H_2O$ was dissolved in 20 mL of deionized water containing 8 mg of hexadecyl trimethyl ammonium bromide (CTAB). Then this solution was rapidly injected into 140 mL of aqueous solution containing 9.08 g 2−methylimidazole and stirred rapidly at room temperature for 40 min, and then stand at room temperature for 12 h. The product was collected by centrifugation, washed by ethanol for three times and dried at 60 °C overnight to obtain ZIF−67 nanocube.

Synthesis of ZIF−67@Cu−Co LDH nanobox: First, 0.4 g ZIF−67 nanocube was dispersed into 80 mL of ethanol. Then 20 mL of ethanol solution containing 0.8 g $Cu(NO_3)_2·3H_2O$ was added drop by drop, and the mixture was put into an ultrasonic bath for 90 min. Finally, the product was collected by centrifugation and washed three times with ethanol, and dried overnight at 60 °C to obtain ZIF−67@Cu−Co LDH

nanobox, called Cu−Co LDH. To change the ratio of Cu and Co, the same amount of ZIF−67 was used as template, and 0.2 g, 0.4 g and 1.2 g of $Cu(NO_3)_2·3H_2O$ were added to obtain Cu−Co_{1-2} LDH, Cu−Co_{1-1} LDH, Cu−Co_{3-1} LDH, respectively.

Synthesis of Cu−Co HNB: The obtained ZIF−67@Cu−Co LDH was used as precursor and further annealed at 400 °C for 2 h at a ramp rate of 1.5 °C/min under a flow of Ar atmosphere to obtain Cu−Co hollow nanobox catalyst (Cu−Co HNB). In addition, Cu−Co $_{1-2}$ HNB, Cu−Co $_{1-1}$ HNB and Cu−Co $_{3-1}$ HNB were prepared with Cu−Co $_{1-2}$ LDH, Cu−Co $_{1-1}$ LDH and Cu−Co $_{3-1}$ LDH as precursor at the same calcination conditions as above, respectively.

Similarly, the ZIF−67@Cu−Co LDH was calcinated at 400 °C, 500 °C and 600 °C to obtain the Cu−Co−400 HNB, Cu−Co−500 HNB and Cu−Co−600 HNB, respectively.

Synthesis of calcined ZIF−67(cal−ZIF−67): The cal−ZIF−67 was prepared by thermal treatment with the pre−prepared ZIF−67 as precursor, under the same conditions as Cu−Co HNB synthesis process.

Synthesis of Cu Co mixture: With 20 mL ethanol as solvent, 0.1 g cal−ZIF−67 and 0.2 g commercial CuO were mixed and ultrasonicated for 60 min, followed by drying to obtain Cu Co mixture.

Synthesis of Cu−Co NPs: 20 mL aqueous solution containing 0.4 g $Cu(NO_3)_2·3H_2O$ and 0.2 g $Co(NO_3)_2·6H_2O$ was added dropwise to Na_2CO_3 solution (0.5 mol/L, 100 mL) with continuous stirring at 60 °C. After stirring for 2 h, the dark solution was cooled to room temperature and then filtered, washed three times with deionized water,

and finally dried overnight at 60 °C. The dried black powder was annealed under the same conditions as above to obtain the Cu−Co NPs.

Synthesis of cathod: A mixture of 10 mg catalysts, 1.25 mg acetylene black and 22 μL PTFE (wt 5%) were mixed adequately and coated on 1×2 cm^2 nickel foam, followed by drying in oven for more than 8 h.

Characterizations

The surface morphology and elemental distribution of electrocatalysts were observed using a field emission scanning electron microscope (SEM, Sigma−300) equipped with an energy dispersive spectrometer (EDS) and transmission electron microscope (TEM, JEOL JEM−2100; Tokyo; Japan) equipped with EDS. The structure composition of the materials was observed by X−ray diffractometer (XRD) (Cu−K−α, 40 kV mA) in a scanning range of 20−80°. X−ray photoelectron spectra (XPS) was observed by the PHI−5300 instrument for identifying the structure composition of catalysts.

Electrochemical tests

The electrochemical properties were evaluated by electrochemical workstation (CHI 660E Shanghai Chenhua). The materials of working electrode was made of active material (10 mg), acetylene black, polytetrafluoroethylene (PTFE, wt 5%) aqueous dispersion at 8:1:1 weight ratio.

Amperpmetric i−t curve, linear sweep voltammetry (LSV), cyclic voltammetry (CV), and electrochemical impedance spectroscopy (EIS) were tested by the three−electrode system in a 100 ppm $NaNO_3$ and 0.1 M Na_2SO_4 solution. Saturated calomel electrode

(SCE) were used as reference electrode and Three−dimensional nickel foam were used as counter electrode. The i−t test was performed at −1.3 V *vs.* SCE. The LSV tests were conducted at 0 to −1.6 V at 10 mV/s scan rate. Tafel slope was derived from LSV with a sweep speed of 10 mV/S. The CV measurements were performed at the range from 0.4 to −1.6 V at 20 mV/s scan rate. Double layer capacitance (C_{dl}) was determined by CV scan at different scan rates (20−100 mV s^{-1}) in a non−Faraday potential window, the plot of capacitive anode and cathode current differences [(j_a−j_c)/2] at a set potential against the CV scan rates show a linear relationship, and the slope was C_{dl}. ECSA is calculated by C_{dl}. The EIS analysis was recorded at 100 mHz to 100 kHz with 5 mV amplitude. The original electrolyte was neutral, and the pH of the solution was adjusted by hydrochloric acid (HCl) and sodium hydroxide (NaOH), respectively. The pH was measured by a pH electrode.

***In situ* differential electrochemical mass spectrometry (DEMS) measurements**

The 100 ppm $NaNO_3$−N and 0.1 M Na_2SO_4 electrolytes are fed into a specially designed electrochemical cell via a peristaltic pump. Ar was continuously bubbled into the electrolyte before and during the dem measurement. A glassy carbon electrode coated with Cu−Co HNB, a platinum wire electrode and a saturated calomel electrode were used as working, counter and reference electrodes, respectively. LSV was tested from 0 to −1.6 V *vs.* SCE at a scan rate of 10 mV s^{-1} until the baseline remained stable. Then, the corresponding mass signal appears. After the electrochemical test ends and the mass signal returns to the baseline, the next cycle begins using the same test conditions to avoid unexpected errors during dem measurements. The experiment was performed for

three consecutive cycles.

Analytical methods

Determination of nitrate and nitrite. In this paper, the ion chromatograph (Soptop IC1820) with anion column (Shanghai Shunyuhengping Company) was used to detect nitrate and nitrite products. The standard curve was drawn by measuring different concentrations of sodium nitrate and sodium nitrite, and the sample concentration could be obtained by comparing the standard curve with the sample. The specific chromatographic parameters were set as follows: the quantitative ring volume of the injection liquid was 20 μL, the eluent was 3.6 mmol·L^{-1} Na_2CO_3 solution, the flow rate was set at 0.6 mL·min^{-1}, and the detection time was 36 min. In order to prevent the error caused by the high concentration of sulfate in the electrolyte, the sample was diluted 10 times for analysis. Nitrate and nitrite peaked at about 23 and 15 min, respectively. The linear fitting equation of the standard curve was shown in Fig. S14.

Determination of ammonia. The concentration of NH_3 produced in the nitrogen reduction reaction was measured by the indophenol blue method. The electrolyte was diluted to an appropriate concentration to match the range of the UV−vis absorption spectrum (TU−1950). First, 2 mL aliquot of the solution was removed from the electrochemical reaction vessel. Then, 2 mL NaOH solution (1 M) containing 5 wt% salicylic acid and 5 wt% sodium citrate was added, and followed by the addition of 1 mL NaClO (0.05 M) and 0.2 mL $C_5FeN_6Na_2O$ (sodium nitroferricyanide, 1 wt%). After one hour at room temperature, the UV−vis absorption spectrum was measured at a wavelength of 500−800 nm. The formation of indophenol blue was determined using

the absorbance at a wavelength of 655 nm. A concentration−absorbance curve was drawn to obtain the standard curve, and the linear equation obtained by linear fitting was used to calculate the ammonia concentration, as shown in Fig. S14.

Determination of copper and cobalt ions. The ICP−OES (ICAP 7000 Series, Thermo Fisher Scientific; Waltham; USA) was applied to test the ions concentration and analyze the leaching of Cu and Co ions from Cu−Co HNB and Cu−Co mixture after 12 h electrocatalytic nitrate reduction were analyzed.

Data analysis

A series of data that can be used to analyze the performance of electrocatalytic denitrification, the selectivity of nitrite ($S_{NO_2^-}(\%)$), ammonia ($S_{NH_4^+}(\%)$)were calculated according to the following equations.

$$S_{NH_4^+}(\%) = \frac{C_t(NH_4^+)}{C_0(NO_3^-) - C_t(NO_3^-)} \times 100\% \quad (1)$$

$$S_{NO_2^-}(\%) = \frac{C_t(NO_2^-)}{C_0(NO_3^-) - C_t(NO_3^-)} \times 100\% \quad (2)$$

The measurement of N_2 was mainly obtained by the substruction method, because the amount of other gas products (NO, N_2O) generated in the electrocatalytic system was very small and could be omitted.

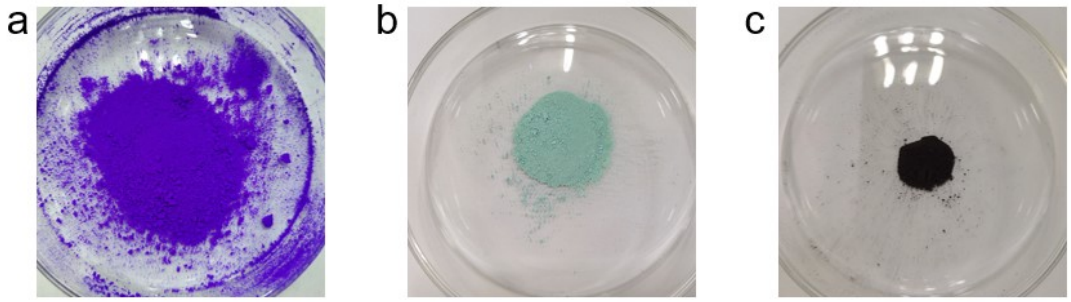

Fig. S1. The digital photograph of key steps. (a) Bright purple ZIF−67; (b) light blue Cu−Co_{2-1} LDH; (c) dark gray Cu−Co_{2-1} HNB.

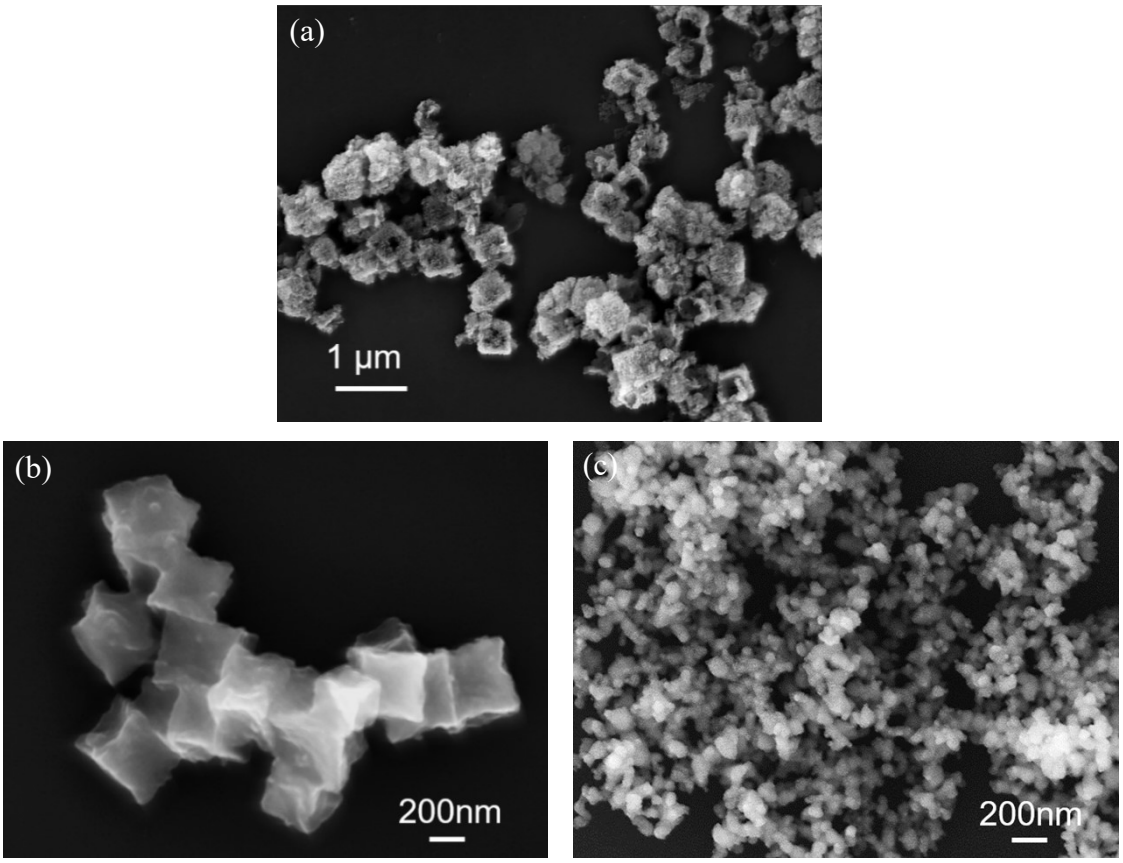

Fig. S2. SEM images of (a) broken Cu−Co_{2-1} LDH nanoparticles, (b) cal−ZIF−67 and (c) commercial CuO nanoparticles.

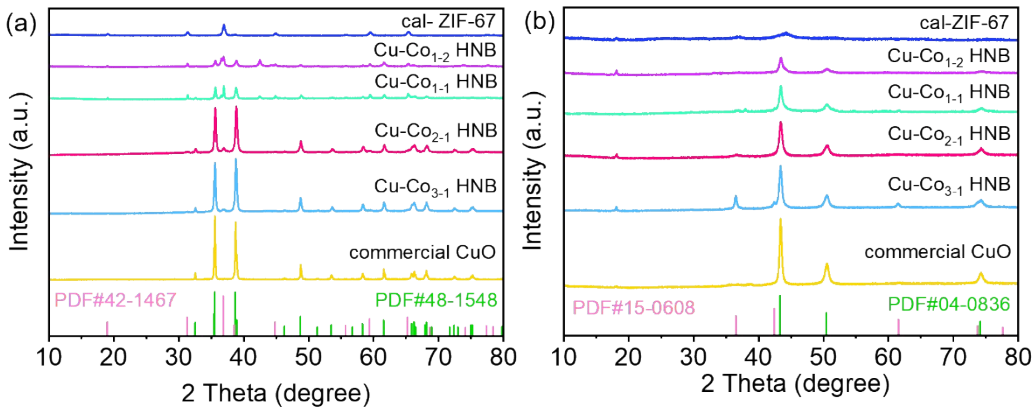

Fig. S3. XRD patterns of the synthesized samples with different mass ratios (a) before and (b) after reduction reaction.

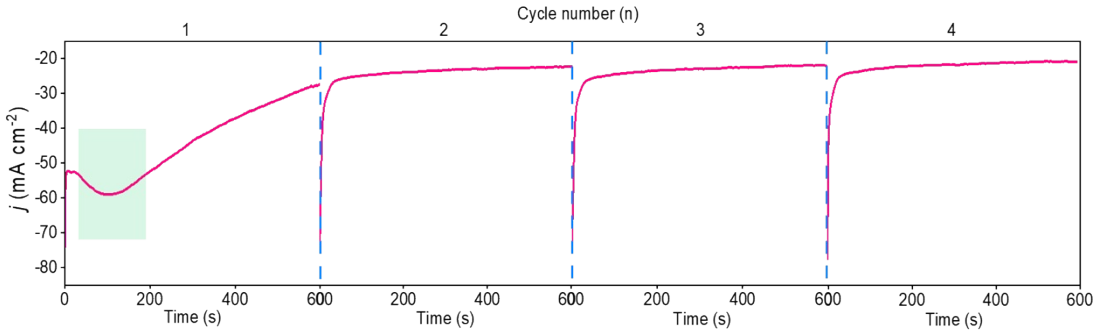

Fig. S4. Chronoamperometry curves of Cu−Co_{2-1} HNB during four consecutive cycling nitrate reduction processes at −1.3 V *vs.* SCE. (100 ppm NO_3^-−N and 0.1 M Na_2SO_4, with agitation, neutral pH)

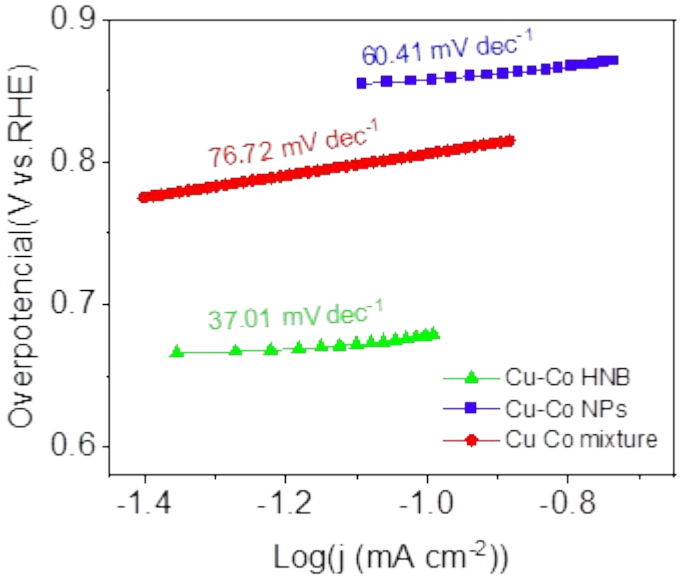

Fig. S5. The LSV−derived Tafel slopes of Cu−Co HNB, Cu−Co NPs and Cu Co mixture.

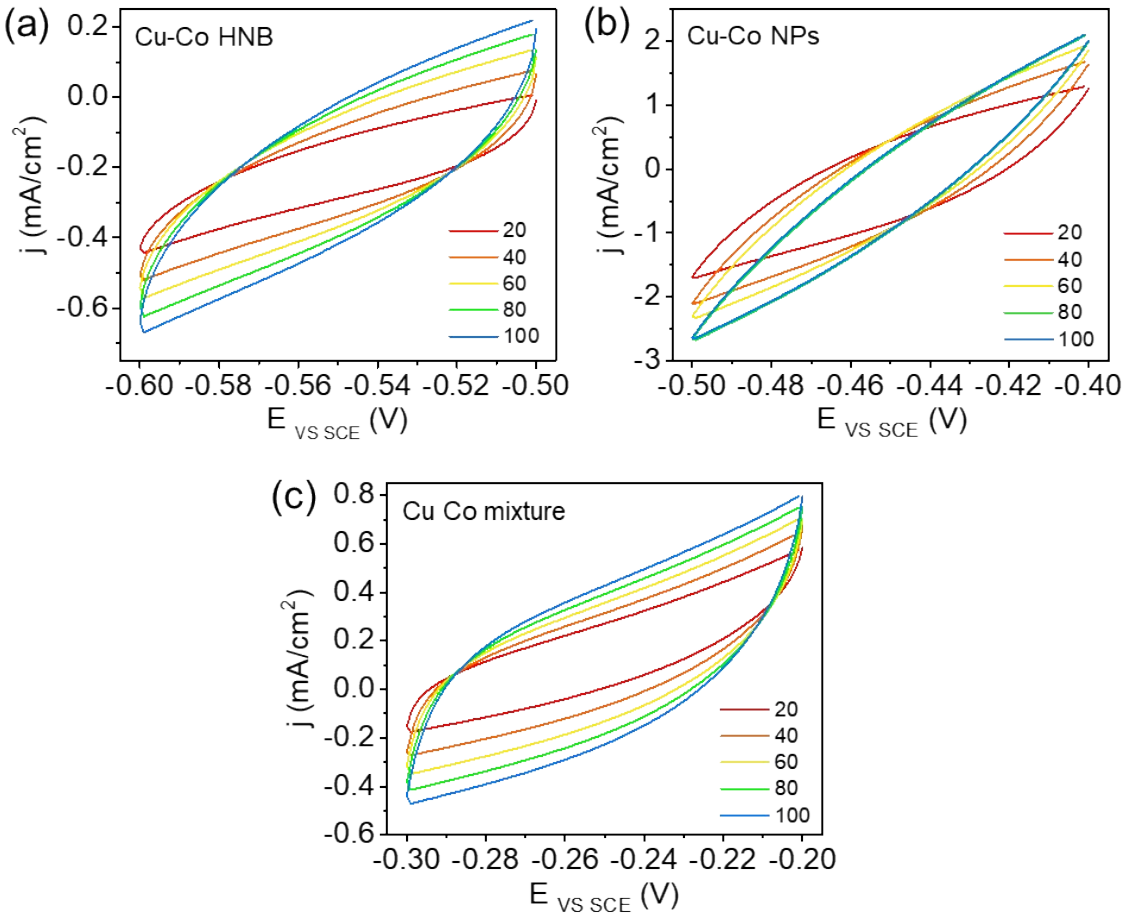

Fig. S6. Determination of the electrochemically active surface area (ECSA) by measuring the double−layer capacitance from cyclic voltammetries obtained at various scan rates (20, 40, 60, 80, and 100 mV/s): (a) Cu−Co HNB, (b) Cu−Co NPs and (c) Cu Co mixture.

The double layer capacitance (C_{dl}) of different materials was determined to be 2.42 mF·cm^{-2} (Cu−Co HNB), 1.52 mF·cm^{-2} (Cu Co mixture) and 0.88 mF·cm^{-2} (Cu−Co NPs). The ECSA was calculated according to the equation: ECSA = C_{dl}/specific capacitance (assuming the specific capacitance of 0.04 mF·cm^{-2}·cm^{-2}). The ECSA of Cu−Co HNB, Cu Co mixture and Cu−Co NPs were 60.5, 38 and 22 cm^2·g$^{-1}_{catalyst}$, respectively.

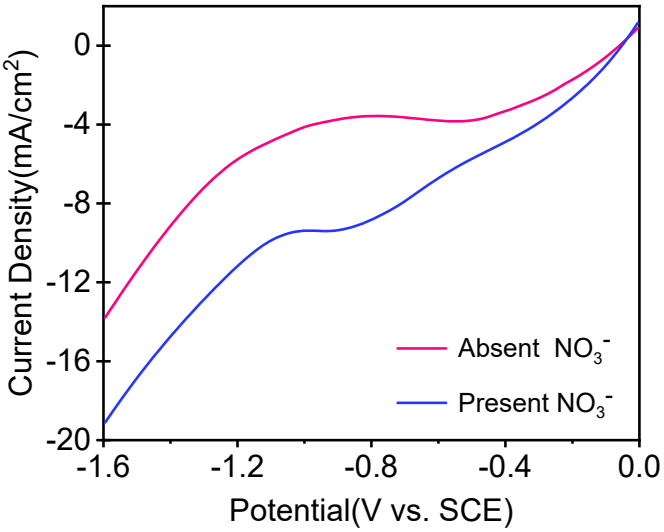

Fig. S7. LSV curves of Cu−Co HNB cathode in the absence and presence of nitrate.

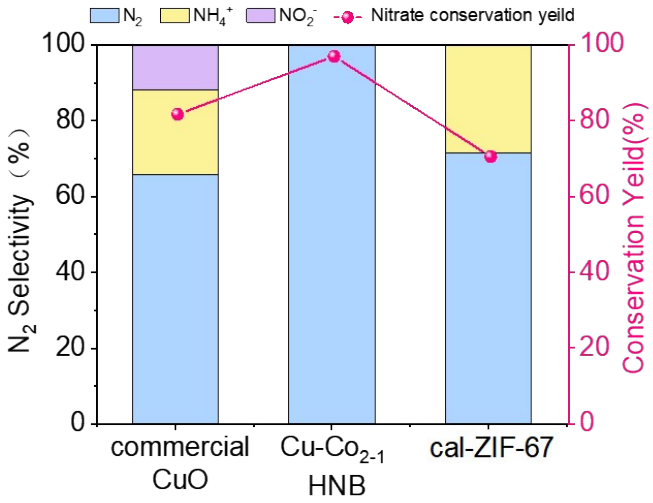

Fig. S8. The change of conversion yield and product selectivity of commercial CuO, Cu−Co_{2-1} HNB and cal−ZIF−67 electrodes in NRR process.

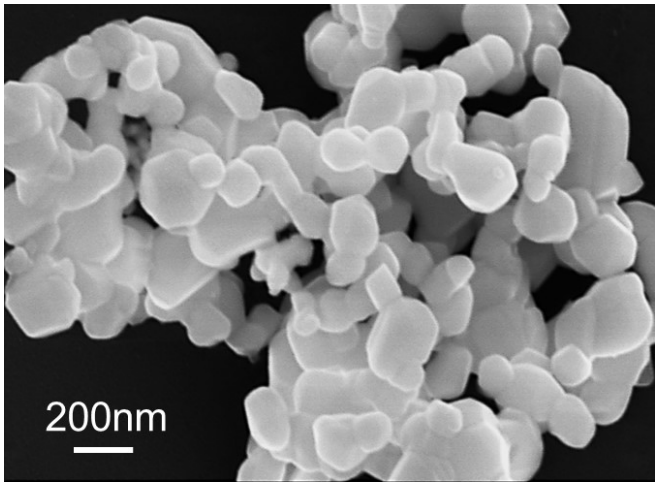

Fig. S9. SEM image of Cu−Co−600 HNB.

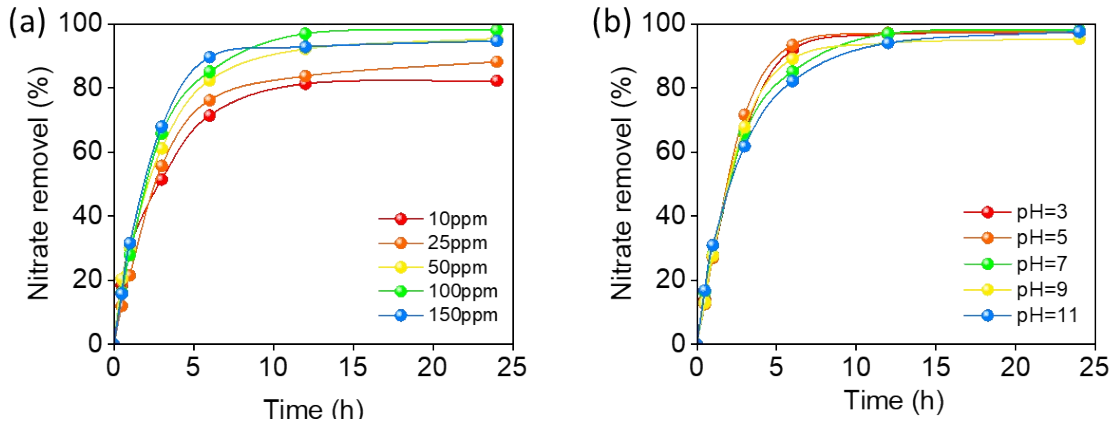

Fig. S10. The conversion rate of NO_3^- in Cu–Co HNB electrocatalytic system at (a) different concentrations of NO_3^-–N and (e) different initial pH.

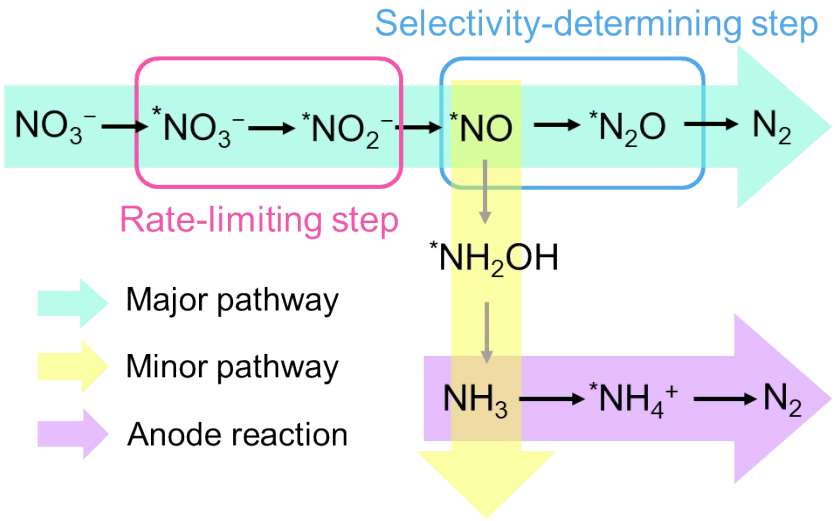

Fig. S11. Nitrate reduction pathway by Cu−Co HNB electrode.

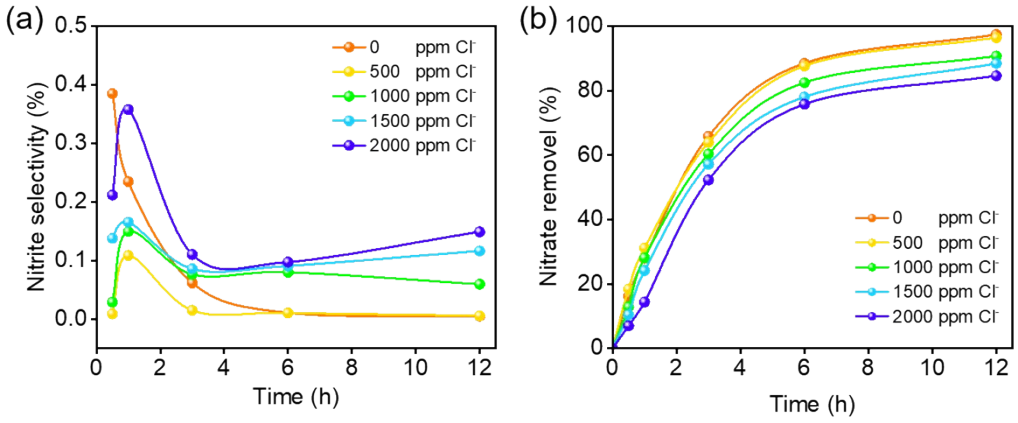

Fig. S12. Effects of different concentrations of Cl^- on (a) the electrocatalytic NO_3^- conversion rate and (b) the products selectivity of NO_2^- within 12 h of Cu-Co HNB.

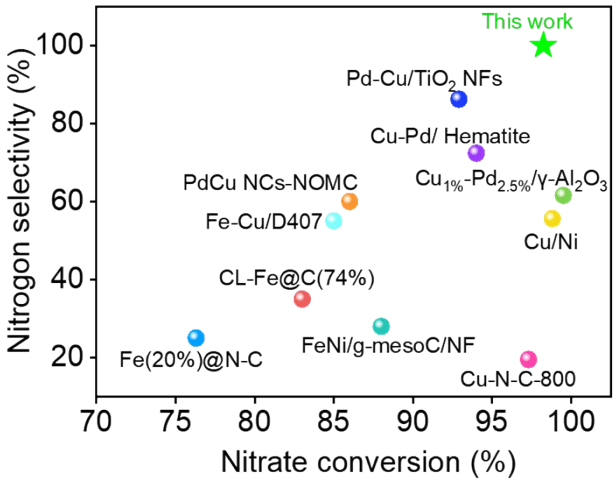

Fig. 13. Performance of different catalysts for electrocatalytic reduction of nitrate in Cl–free systems.

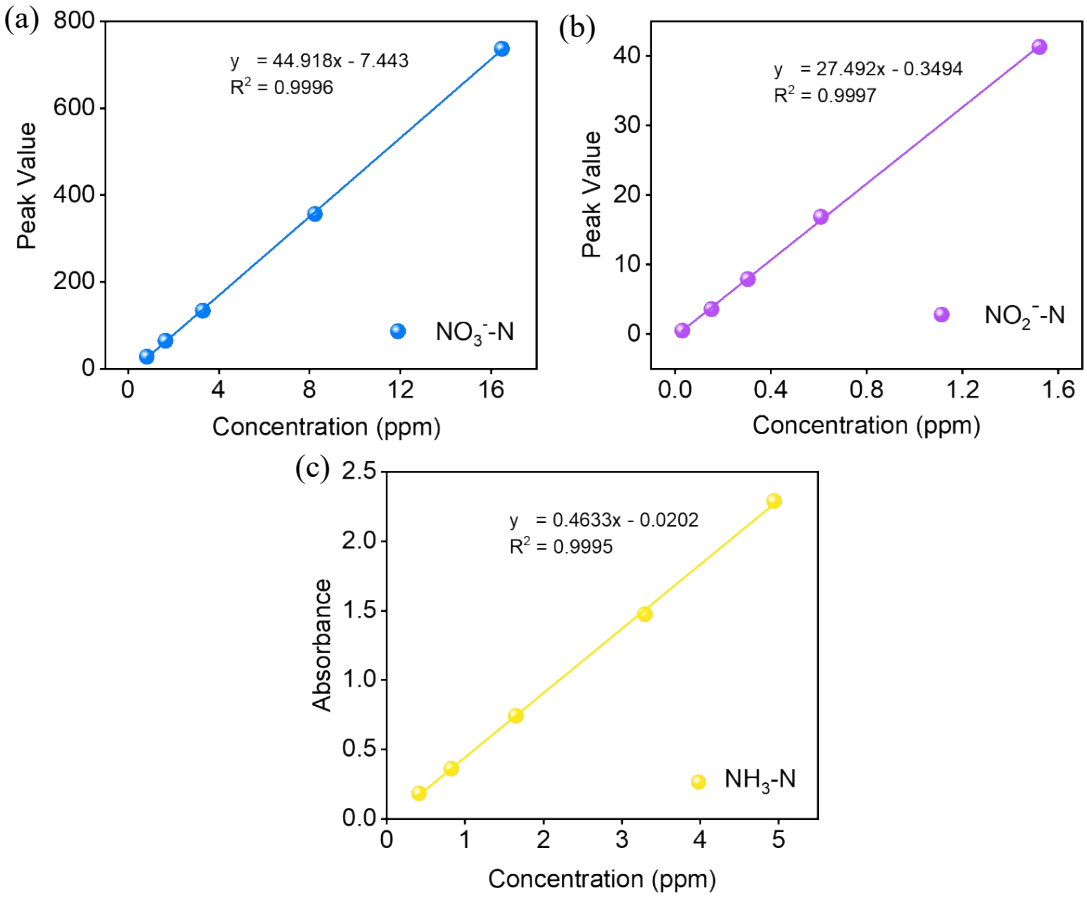

Fig. S14. Concentration standard curve of (a) NO_3^-–N, (b) NO_2^-–N, (c) NH_3–N.

Table S1. Electrocatalytic reduction performance of Cu−Co HNB with different Cu−Co mass ratios.

Electrocatalyst	Nitrate Removal (%)	N_2 Selectivity (%)	NH_4^+ Selectivity (%)	NO_2^- Selectivity (%)
Cu−Co_{3-1} HNB	97.7704	99.9727	0.02442	0.00288
Cu−Co HNB	98.14277	99.99881	0	0.00119
Cu−Co_{1-1} HNB	92.01691	73.31165	26.62835	0.06
Cu−Co_{1-2} HNB	88.7046	11.38611	88.61012	0.00377
cal−ZIF−67	70.54059	71.37246	28.60755	0.01999
commercial CuO	81.7036	65.63637	22.57671	11.78692

Table S2. Electrocatalytic reduction performance of Cu−Co HNB calcined at different temperatures.

Temperature（°C）	Nitrate Removal (%)	N_2 Selectivity (%)	NH_4^+ Selectivity (%)	NO_2^- Selectivity (%)
Cu−Co−400 HNB	98.1428	99.9988	0	0.00119
Cu−Co−500 HNB	97.9881	99.9727	0.01215	0.015151
Cu−Co−600 HNB	90.0932	51.2996	48.6257	0.074783

Table S3. Electrocatalytic reduction performance of Cu−Co HNB at different concentrations of NO_3^-−N.

C_0 (NO_3^-−N) (ppm)	Nitrate Removal (%)	N_2 Selectivity (%)	NH_4^+ Selectivity (%)	NO_2^- Selectivity (%)
10	82.33981	98.84064	0.83979	0.31957
25	88.84179	98.1373864	1.798542	0.064071
50	95.55573	99.75253	0.24266	0.00481
100	98.1428	99.9988	0	0.00119
150	92.93605	67.38297	32.55954	0.05749

Table S4. Electrocatalytic reduction performance of Cu−Co HNB at different initial pH.

Initial pH value	Nitrate Removal (%)	N_2 Selectivity (%)	NH_4^+ Selectivity (%)	NO_2^- Selectivity (%)
3	97.25613	28.96935	71.01129	0.01935
5	97.77919	15.03358	84.96403	0.00239
7	98.14277	99.99881	0	0.00119
9	95.42188	91.30402	7.67801	1.01797
11	97.64419	98.53092	0.88095	0.58813

Table S5. The change of nitrate conversion yield and product selectivity of Cu−Co HNB, Cu−Co NPs and Cu Co mixture electrocatalytic systems in 12 h.

Electrocatalyst	Nitrate Removal (%)	N_2 Selectivity (%)	NH_4^+ Selectivity (%)	NO_2^- Selectivity (%)
Cu−Co HNB	98.1428	99.9988	0	0.00119
Cu−Co NPs	89.3659	88.8167	11.1076	0.07564
Cu Co mixture	77.6602	55.2942	43.7592	0.94658

Table S6. Nitrate removal efficiency and the selectivity of nitrogen in the presence of TBA.

Time (h)	Nitrate Removal (%)	N_2 Selectivity (%)	NH_4^+ Selectivity (%)	NO_2^- Selectivity (%)
0.5	10.2184	39.7468	8.0589	52.1943
1	20.7599	18.9322	15.9033	65.1645
3	56.3003	33.8787	7.3446	58.7767
6	74.9493	53.8234	25.6451	20.5316
12	79.9971	78.4164	7.1918	14.3918

Table S7. Reusability of Cu−Co HNB electrode.

Cycles	Nitrate Removal (%)	N_2 Selectivity (%)	NH_4^+ Selectivity (%)	NO_2^- Selectivity (%)
1	98.1428	99.9988	0	0.00119
2	97.8295	99.89218	0.088041	0.019782
3	96.66177	94.32062	5.542381	0.136999
4	93.0707	90.18784	9.648222	0.163938
5	95.66916	92.21453	7.711579	0.073891

Table S8. Effect of different Cl^- contents on electrocatalytic reduction performance of Cu-Co HNB for 12h.

C_0 (Cl^-) (ppm)	Nitrate Removal (%)	N_2 Selectivity (%)	NH_4^+ Selectivity (%)	NO_2^- Selectivity (%)
0	98.1428	99.9988	0	0.00119
500	96.48825	99.99445	0	0.00555
1000	90.77542	99.93514	0.00539	0.05948
1500	88.45932	99.87523	0.00829	0.11647
2000	84.65799	99.83659	0.01444	0.14897

Table S9. Summary of nitrate conversion efficiency of different catalysts.

Materials	$C_0(NO_3^-–N)$ (ppm)	Electrolyte	Nitrate removal (%)	Nitrogen selectivity (%)	Ref.
Cu/Fe@NCNFs−700	100	0.02 M NaCl+0.1 M Na_2SO_4	76	94	2
Ni/Fe_3O_4	50	0.01 M NaCl	90.2	88.8	3
nZVI/OMC	50	0.02 M NaCl	67	74	4
Ni−TNTA	50	0.3 g L^{-1} NaCl+0.5 g L^{-1} Na_2SO_4	89.6	~100	5
CL−Fe@C(74%)	50	0.02 M NaCl	50	50	6
		0.1 M Na_2SO_4	83	35	
FeNi/g−mesoC/NF	50	0.02 M NaCl+0.05 M Na_2SO_4	75	100	7
		0.05 M Na_2SO_4	88	28	
$Co_3O_4–TiO_2/Ti$	50	1000 ppm Cl^-+0.1 M Na_2SO_4	60	71	8
Fe(20%)@N−C	50	1 g L^{-1} NaCl+0.05 M Na_2SO_4	83	100	9
		0.05 M Na_2SO_4	76.3	25	
Fe−Cu/D407	50	/	85	55	10
Cu/Ni	50	0.1 M Na_2SO_4	99	55.6	11
Cu−N−C−800	50	0.05 M Na_2SO_4	97.3	19.5	12
PdCu NCs−NOMC	100	0.1 M Na_2SO_4	86	60	13
Cu−Pd/ Hematite	30	/	94	72.4	14
Pd−Cu/TiO_2 NFs	30	/	92.9	86.2	15
$Cu_{1\%}$(900 °C)−$Pd_{2.5\%}/\gamma–Al_2O_3$	50	0.05 M Na_2SO_4	100	61.56	16
Cu−Co HNB	100	0.1 M Na_2SO_4	98.1	~100	This work

Reference:

1. H. Hu, B. Y. Guan and X. W. Lou, Construction of complex CoS hollow structures with enhanced electrochemical properties for hybrid supercapacitors, *Chem*, 2016, **1**, 102-113.
2. Y. Lan, H. Luo, Y. Ma, Y. Hua, T. Liao and J. Yang, Synergy between copper and iron sites inside carbon nanofibers for superior electrocatalytic denitrification, *Nanoscale*, 2021, **13**, 10108-10115.
3. Z. A. Jonoush, A. Rezaee and A. Ghaffarinejad, Electrocatalytic nitrate reduction using Fe^0/Fe_3O_4 nanoparticles immobilized on nickel foam: Selectivity and energy consumption studies, *J. Cleaner Prod.*, 2020, **242**, 118569.
4. W. Teng, N. Bai, Y. Liu, Y. Liu, J. Fan and W. X. Zhang, Selective nitrate reduction to dinitrogen by electrocatalysis on nanoscale iron encapsulated in mesoporous carbon, *Environ. Sci. Technol.*, 2018, **52**, 230-236.
5. F. Liu, K. Liu, M. Li, S. Hu, J. Li, X. Lei and X. Liu, Fabrication and characterization of a Ni-TNTA bimetallic nanoelectrode to electrochemically remove nitrate from groundwater, *Chemosphere*, 2019, **223**, 560-568.
6. L. Su, D. Han, G. Zhu, H. Xu, W. Luo, L. Wang, W. Jiang, A. Dong and J. Yang, Tailoring the assembly of iron nanoparticles in carbon microspheres toward high-performance electrocatalytic denitrification, *Nano Lett.*, 2019, **19**, 5423-5430.
7. X. Chen, T. Zhang, M. Kan, D. Song, J. Jia, Y. Zhao and X. Qian, Binderless and oxygen vacancies rich FeNi/graphitized mesoporous carbon/Ni foam for electrocatalytic reduction of nitrate, *Environmental Science & Technology*, 2020, **54**, 13344-13353.
8. J. Gao, B. Jiang, C. Ni, Y. Qi, Y. Zhang, N. Oturan and M. A. Oturan, Non-precious Co_3O_4-TiO_2/Ti cathode based electrocatalytic nitrate reduction: Preparation, performance and mechanism, *Appl. Catal. B Environ.*, 2019, **254**, 391-402.
9. W. Duan, G. Li, Z. Lei, T. Zhu, Y. Xue, C. Wei and C. Feng, Highly active and durable carbon electrocatalyst for nitrate reduction reaction, *Water Res.*, 2019, **161**, 126-135.
10. T. Tang, Q. Xing, S. Zhang, Y. Mu, X. Jiang, Z. Zhou, X. Xiao and J. Zou, High selective reduction of nitrate into nitrogen by novel Fe-Cu/D407 composite with excellent stability and activity, *Environ. Pollut.*, 2019, **252**, 888-896.
11. Y. Shih, Z. Wu, Y. Huang and C. Huang, Electrochemical nitrate reduction as affected by the crystal morphology and facet of copper nanoparticles supported on nickel foam electrodes (Cu/Ni), *Chem. Eng. J.*, 2020, **383**, 123157.
12. T. Zhu, Q. Chen, P. Liao, W. Duan, S. Liang, Z. Yan and C. Feng, Single-atom Cu catalysts for enhanced electrocatalytic nitrate reduction with significant alleviation of nitrite production, *Small*, 2020, **16**, 2004526.
13. H. Xu, H. Xu, Z. Chen, X. Ran, J. Fan, W. Luo, Z. Bian, W. X. Zhang and J. Yang, Bimetallic pdcu nanocrystals immobilized by nitrogen-containing

ordered mesoporous carbon for electrocatalytic denitrification, *ACS Appl. Mater. Interfaces*, 2019, **11**, 3861-3868.

14. S. Jung, S. Bae and W. Lee, Development of Pd-Cu/hematite catalyst for selective nitrate reduction, *Environ. Sci. Technol.*, 2014, **48**, 9651-9658.
15. Q. Wang, W. Wang, B. Yan, W. Shi, F. Cui and C. Wang, Well-dispersed Pd-Cu bimetals in TiO_2 nanofiber matrix with enhanced activity and selectivity for nitrate catalytic reduction, *Chem. Eng. J.*, 2017, **326**, 182-191.
16. F. Shi, J. Li, J. Liang, C. Bao, J. Gu, K. Li and J. Jia, Highly dispersed Pd-Cu bimetallic nanocatalyst based on γ-Al_2O_3 combined with electrocatalytic in-situ hydrogen production for nitrate hydroreduction, *Chem. Eng. J.*, 2022, **434**, 134748.